HAL open science

Model based object localization and shape estimation using electric sense on underwater robots

Stéphane Bazeille, Vincent Lebastard, Sylvain Lanneau, Frédéric Boyer

▶ To cite this version:

Stéphane Bazeille, Vincent Lebastard, Sylvain Lanneau, Frédéric Boyer. Model based object localization and shape estimation using electric sense on underwater robots. IFAC 2017: 20th IFAC World Congress, Jul 2017, Toulouse, France. 10.1016/j.ifacol.2017.08.941 . hal-01503876

HAL Id: hal-01503876
https://hal.science/hal-01503876

Submitted on 11 Apr 2017

HAL is a multi-disciplinary open access archive for the deposit and dissemination of scientific research documents, whether they are published or not. The documents may come from teaching and research institutions in France or abroad, or from public or private research centers.

L'archive ouverte pluridisciplinaire **HAL**, est destinée au dépôt et à la diffusion de documents scientifiques de niveau recherche, publiés ou non, émanant des établissements d'enseignement et de recherche français ou étrangers, des laboratoires publics ou privés.

Model based object localization and shape estimation using electric sense on underwater robots

Stéphane Bazeille * , **Vincent Lebastard** * , **Sylvain Lanneau** *
and Frédéric Boyer *

* *DAPI/IRCCYN, Ecole des Mines de Nantes, France*

Abstract: Recently, biologists have shown that the weakly electric fish are able to estimate the electric nature, the localization and the 3D geometric properties of an object using active electric sense. Incredibly, the *Gnathonemus petersii* performs this task in the dark only by moving towards and around the object, its vision is not required. In this paper, we proposed to address the challenging issue of object localization and shape estimation using a real underwater robot equipped with artificial electric sense. To that end, we used a corrected version of the dipolar tensor dedicated to small objects [Ammari et al., 2014] able to capture the electric response of big objects (typically objects whose size is about the one half of the robot length $<$ 10cm). The principal contribution consists in the development of a multi-scale exhaustive search algorithm based on this tensor that allows to estimate in a same step the localization, orientation and shape of an object from electric currents measured along a given trajectory close to the object. Over 108 experiments, our method shows good results as on average we obtained 18% of shape error, 25° of orientation error and 1cm of localization error within a range of $[5, 11]$cm distance with the robot. These results are promising since the problem solved is known to be complex localization and shape being intricately linked in the electrical measurements [Rasnow, 1996].

Keywords: Object localization, Shape estimation, Electric sensing, Modelization, Bio-robotics.

1. CONTEXT OF THE STUDY

1.1 Weakly electric fish

Electric sense is a bio-inspired sensorial ability. It has been observed almost exclusively in aquatic or amphibious animals [Bullock and Heiligenberg, 1986]. Several species of fish have this capacity to sense changes in electric fields in their vicinity. Among fishes, we can distinguish two typical modes of electro-perception: some fish passively sense changes in the nearby electric fields (passive electric sense [Bullock and Heiligenberg, 1986]), while others generate their own weak electric fields and sense its distortions with their skins (active electric sense) [Caputi et al., 1998]. Here, we will only consider the active modality of electric sense. The fish that use active electric sense are called weakly electric fish. These fish are principally nocturnal and live in confined turbid waters of the equatorial forests [Lissmann and Machin, 1958]. In such environments, waters are generally rich in suspended particles (turbib) and cluttered with a lot of plant roots or trees. In these harsh conditions, these fish use electric sense to avoid obstacles while navigating, to communicate with conspecifics, or to hunt their preys. Technically, electric fish perceive their environment by self-generating an electric field thanks to an electric organ located at the base of the tail, and by measuring the distortions of this field through a dense array of electro-receptors distributed over their skin. Electric sense is an omnidirectional short range sense (typical range equal to 1 fish length) that provides to the fish a lot of information about their environment. Behavioral experiments have shown that these fish can discriminate the size and the shape of objects in the dark. In particular, in [von der Emde et al., 1998], biologists demonstrated that when perceiving an object a fish first identifies its electric nature, then localizes the object and finally recognizes the shape. This behavior is astonishing as it has been shown that using electric sense the separation between localization and object geometric properties is not obvious at all. Indeed, localization and shape are both contained in the electrical measurements but are mixed together in a non linear relationship as shown in [Rasnow, 1996]. As an example, a small sphere close to the fish can produce the same electric response as a bigger one located further.

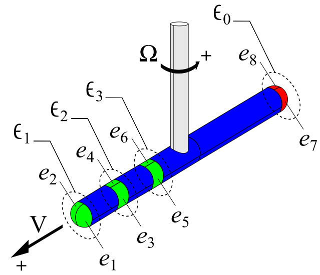

Fig. 1. Our robot equipped with 4 pairs of electrodes.

⋆ This project is supported by the European Unions Horizon 2020 research and innovation program under the grant agreement No 640967. Project subCULTron: http://www.subcultron.eu.

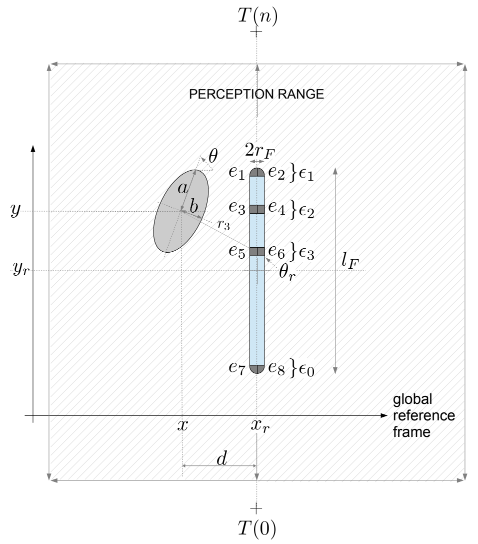

Fig. 2. Experimental set up with our notations.

1.2 Robot equipped with electric sense

Electric sense is a short range omnidirectional perceptual ability ideally suited for muddy/turbib waters and confined underwater environments, i.e. in conditions in which our today underwater perception devices such as vision and sonar are useless. The first, because turbidity decreases the visibility, the second because multiple echoes make the measured signals difficult to interpret. Few artificial electric sensors inspired by weakly electric fish exist today [Bai et al., 2012, Servagent et al., 2013, Dimble et al., 2014, Truong et al., 2015]. In the paper we will use the device presented in [Servagent et al., 2013]. The robot is designed as a long and thin plastic cylinder (length $l_F = 22$cm and radius $r_F = 1$cm), on which 4 pairs of conductive electrodes are arrayed. Among reasons, the slender shape of sensor has been chosen to provide a simple model [Boyer et al., 2012] and ensures the electric field to exhibit a dipolar shape mimicking that of the fish. The electric field is generated by setting a voltage U on the 2 tail electrodes (considered as the emitter) while the 6 others electrodes (considered as receivers) are grounded. The voltage ($U = 10$V at 22kHz) is imposed through an off-board sine wave generator. Note here that a continuous voltage would generate an undesirable electrolysis. Then, the currents that flow across the 6 receivers are measured with an ampere-meter circuit.We note I_k the measure on the electrode e_k that belongs to the macro-electrode ϵ_K (see Fig. 1). Here, we restrict the measure to the amplitude of the electric current, the phase is not considered.

1.3 Definition of the measurement vector

The 6 measured currents are not used directly. In order to facilitate the robot control and to obtain more information about the surroundings of the robot, we use an electric measurement vector denoted M and defined as:

$$M = \begin{pmatrix} I_{lat} \\ \delta I_{ax} \end{pmatrix}, \tag{1}$$

$$\text{with } I_{lat} = \begin{pmatrix} I_{lat,1} \\ I_{lat,2} \\ I_{lat,3} \end{pmatrix} = \begin{pmatrix} I_1 - I_2 \\ I_3 - I_4 \\ I_5 - I_6 \end{pmatrix}, \tag{2}$$

$$\text{and } \delta I_{ax} = \begin{pmatrix} \delta I_{ax,1} \\ \delta I_{ax,2} \\ \delta I_{ax,3} \end{pmatrix} = \begin{pmatrix} (I_1 + I_2 - I^0_{ax,1})/2 \\ (I_3 + I_4 - I^0_{ax,2})/2 \\ (I_5 + I_6 - I^0_{ax,3})/2 \end{pmatrix}. \tag{3}$$

I_{lat} (or "lateral current") represents the differential part of left and right currents. The I^0_{ax} stand for the "basal current", that is to say the current measured without any perturbation and δI_{ax} ("or axial current") represents the common part of the left and right currents flowing across each ϵ_i. As explained in [Boyer et al., 2012], the vector of axial currents δI_{ax} models the variations of the total resistance of the scene while its lateral counterparts I_{lat} is proportional to the lateral incident field. From these considerations, δI_{ax} allows to determine if the object is conductive or insulating, and I_{lat} allows to determine whether the object is on the left or on the right side of the sensor. As a particular case, when $I_{lat} = 0$, the sensor axis is necessarily aligned along the incident field.

2. PROBLEM STATEMENT

2.1 Problem definition

In this paper, we concentrate our efforts on the cognitive tasks of localizing and estimating the shape of an object using active electric sense. The considered scene is composed of 1 static object and 1 robot moving along a trajectory (from $T(0)$ to $T(n)$) and at a distance d with respect to the object (see Fig. 2).Our robot is controlled by its forward velocity V and its angular yaw velocity Ω. In the following, we consider that we have at our disposal an accurate measure of these control inputs. In [Khairuddin and Lionheart, 2016, Ammari et al., 2014], authors show that at leading order, the electric response of any shaped object can be described as that of an ellipsoid. Therefore, objects are described by ellipsoids and their electrical response are modeled analytically by their first order generalized polarization tensor [Ammari et al., 2014]. Due to experimental constraints which prevent us from measuring the object influence only (the aquarium walls were perceived by the robot because of its smallness), all experiments were performed twice with and without object to be able to remove the effects of the aquarium. For this reason, for all experiments, the robot trajectory has been deliberately chosen as a simple straight line alongside the object according to the simple control law:

$$V = C \text{ and } \Omega = 0, \quad \text{with } C \text{ a constant.} \tag{4}$$

In the global reference frame, the robot pose $T(k)$ will be defined as: x_r, y_r, θ_r with $k \in [1, n]$.

2.2 Mathematical definition

We search for the object O (defined by its electric conductivity, localization, and shape) that disturbs the electric field generated by the robot. Moreover, we will do the following assumptions:

- the water conductivity γ is perfectly known and uniform,
- the displacement of the robot is known at each currents measurement,
- the object can be modeled as a prolate ellipsoid (i.e. axisymmetric about its major axis) whose length is smaller than a half of the sensor length.

Under these experimental conditions, the object O (named "real object") is entirely described by 6 parameters: its localization (x, y) and its orientation (θ) in the global frame of reference, its semi-axis (a, b) and its electric conductivity σ. The third semi-axis of the ellipsoid is equal to the second one. All these parameters are constrained in the following intervals:

- $x, y \in [-l_F, l_F]$ (limited by the perception range),
- $\theta \in [0, \pi/2]$,
- $a, b \in [0, l_F/4]$ with $a \geq b$,
- $\sigma \in \{1e^5, 1e^{-5}\}$.

Giving the fact that the parameters are constrained in small intervals and that we dispose of an analytical model able to predict the measured currents imaging a given scene (see Section 3), we propose to address the inverse problem of object localization and estimation by using a greedy algorithm that tests all possible direct models while selecting the optimal solution. It has to be noted that to obtain an accurate approximation of the ellipse parameters a discriminative robot motion along the object is essential. In the rest of the paper, we suppose that we test m candidates among which $O_0 = (x_0, y_0, \theta_0, a_0, b_0, \sigma_0)$ is the best one.

3. MODELIZATION OF ELECTRIC SENSE

3.1 The analytical model for our slender robot

Assuming that we used the robot presented in the previous section ($l_F = 22$cm and $r_F = 1$cm), we derived an analytical model of the electrical response of an object based on its leading order dipolar tensor [Boyer et al., 2012]. The model considers that the object is small enough to assume the electric field as uniform on its domain.Such a model has given good recognition results in simulation with such small objects [Lanneau et al., 2016]. For a given scene, the currents measured on the receiving electrodes is given by:

$$I_{lat}(T(k), O_x) = \frac{1}{4\pi}.P_\perp.H.R_{\theta_s}.P.R_{\theta_s}^t.G^t.C_0.U, \qquad (5)$$

$$\delta I_{ax}(T(k), O_x) = \frac{1}{4\pi\gamma}.C_0.G.R_{\theta_s}.P.R_{\theta_s}^t.G^t.C_0.U, \qquad (6)$$

where I_{lat}, δI_{ax} are vectors of currents 4×1, C_0 is a 4×4 matrix encoding the robot morphology and conductivity, $P_\perp$ is a 4×4 diagonal matrix depending on the polarization of the electrodes, R_{θ_s} is a rotation matrix depending on the angle between the sensor and the object $\theta_s = \theta - \theta_r$, P a 3×3 diagonal matrix modeling the ellipsoid object electric response (called tensor), G and H are 4×3 matrices encoding the distance between the object center and the electrodes, and U is the 4×1 polarization vector encoding the voltage imposed to the emitting electrodes with respect to the receiving ones. In [Boyer et al., 2012], $P_\perp, C_0, U, G$, H are defined by:

$$P_\perp = \begin{pmatrix} 5.29e-4 & 0 & 0 & 0 \\ 0 & 6.74e-4 & 0 & 0 \\ 0 & 0 & 6.95e-4 & 0 \\ 0 & 0 & 0 & 5.52e-4 \end{pmatrix},$$

$$C_0 = \gamma. \begin{pmatrix} 0.07653 & -0.03152 & -0.02318 & -0.02184 \\ -0.03122 & 0.08393 & -0.03199 & -0.02071 \\ -0.02292 & -0.03206 & 0.07803 & -0.02304 \\ -0.02182 & -0.02090 & -0.02333 & 0.06605 \end{pmatrix}.$$

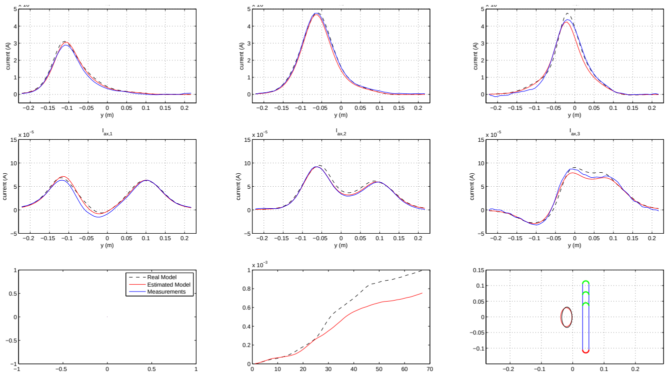

Fig. 3. Experiment using Ammari tensor with a conductive ellipsoid 33×16mm with $\theta_s = 0°$, $d = 70$mm. For all plots, experimental measurements are in blue, model measurements with the real object are in dotted black, and model measurements with the estimated object are in red. 1) $I_{lat,1}$ 2) $I_{lat,2}$, 3) $I_{lat,3}$ 4) $\delta I_{ax,1}$ 5) $\delta I_{ax,2}$, 6) $\delta I_{ax,3}$, 7) Legend 8) Scores 9) Result.

$$U = \begin{pmatrix} 0 \\ 0 \\ 0 \\ U_0 \end{pmatrix}, \qquad G = \begin{pmatrix} \frac{x_c - x_1}{r_1^3} & \frac{y_c}{r_1^3} & 0 \\ \vdots & \vdots & \vdots \\ \frac{x_c - x_4}{r_4^3} & \frac{y_c}{r_4^3} & 0 \end{pmatrix},$$

$$H = \begin{pmatrix} \frac{3y_c(x_c - x_1)}{r_1^5} & \frac{2y_c^2 - (x_c - x_1)^2}{r_1^5} & 0 \\ \vdots & \vdots & \vdots \\ \frac{3y_c(x_c - x_4)}{r_4^5} & \frac{2y_c^2 - (x_c - x_4)^2}{r_4^5} & 0 \end{pmatrix},$$

with $r_{k=1...4} = \sqrt{(x_c - x_k)^2 + (y_c)^2}$, x_k the axial coordinates of the electrode e_k and x_c, y_c the object center position in the sensor frame (see Fig. 2).

3.2 Expression of the ellipse tensor [Ammari et al., 2014]

As shown in [Ammari et al., 2014], at the leading order the electric response of an object can be modeled by the following tensor:

$$P = V. \begin{pmatrix} \lambda_1(\eta) & 0 & 0 \\ 0 & \lambda_2(\eta) & 0 \\ 0 & 0 & \lambda_2(\eta) \end{pmatrix},$$

with $V = 4/3.\pi.a.b^2$ the object's volume, $\eta = a/b$ its aspect ratio, and λ_1, λ_2 defined as:

- $(\lambda_1, \lambda_2) = (1/A, 1/B)$ for conductive objects,
- $(\lambda_1, \lambda_2) = (1/(A-1), 1/(B-1))$ for insulating objects.

where we introduced the elliptic integrals A, B as:

$$\begin{cases} A(\eta) = \eta^{-2} \int_1^{+\infty} \frac{1}{t^2\,(t^2 - 1 + \eta^{-2})} dt, \\ B(\eta) = \eta^{-2} \int_1^{+\infty} \frac{1}{(t^2 - 1 + \eta^{-2})^2} dt. \end{cases} \qquad (7)$$

For a sphere (i.e. $a = b$), which is a particular case of the ellipse we have $\lambda_1 = \lambda_2 = \chi.a^3$ with a the radius of the sphere, and χ a contrast factor. $\chi = 1$ for conducting objects and $\chi = -1/2$ for insulating objects. Moreover, as the sphere is isotropic, R and R^t can be removed in Eq. 5,6.

On Fig. 3 we present a first illustration of localization and shape estimation using this ellipse tensor for an ellipsoid of size 33×16mm with $\theta_s = 0$. This figure shows the good approximation of the 6 M_i in comparison with the real experimental measurements. The score evolutions for the real object (black) compare to the estimated one (red) are shown on subplot 8 and the result is shown on subplot 9.

4. OBJECT LOCALIZATION AND ESTIMATION

4.1 Developed approach

Our method can be structured into 2 stages. First, the recognition of the electric conductivity of the object and its side with respect to the robot is performed. Second, the estimation of its localization and of its geometric properties is done.

Stage 1: Detect the object, find σ_0 and sensor side on which the object is. Since the sensor goes forward, it discovers its environment with its front head electrodes. While $\delta I_{ax,1} = 0$ the robot do not perceive the object so we do not use the measurements. When $\delta I_{ax,1} \neq 0$, depending on its sign we extract the electric conductivity of the object σ_0. Then from σ_0, the side of the object is found depending on the sign of $I_{lat,1}$ as shown in [Lebastard et al., 2016] where the following scenarios were listed:

- $\delta I_{ax,1}, I_{lat,1} > 0$ it is conducting on the left,
- $\delta I_{ax,1}, I_{lat,1} < 0$ it is insulating on the left,
- $\delta I_{ax,1} > 0, I_{lat,1} < 0$ it is conducting on the right,
- $\delta I_{ax,1} < 0$, $I_{lat,1} < 0$ it is insulating on the right,
- $\delta I_{ax,1} > 0$, $I_{lat,1} = 0$ it is conducting facing the robot,
- $\delta I_{ax,1} < 0$, $I_{lat,1} = 0$ it is insulating facing the robot.

Stage 2: Estimate the 5 unknown parameters: x_0, y_0, θ_0, a_0 and b_0. Giving the object electric conductivity and its side with respect to the robot, while we perceive the object we continue the localization and the shape estimation. This estimation requires from the user the 3 discretization parameters $\epsilon_{xy}, \epsilon_\theta, \epsilon_{ab}$ that divide the research space defined in Section 2.2. Then, for O_m an object candidate, $T(k)$ a pose of the robot $(x_{r,k}, y_{r,k}, \theta_{r,k})$ on the trajectory T, our model computes a vector of 6 estimated currents through the function f (see Eq. 8). Supposing n to be the number of points along the trajectory, we have $\forall k \in [1, n]$,

$$f(T(k), O_m) = \widehat{M(k)} = \begin{pmatrix} I_{lat}(T(k), O_m) \\ \delta I_{ax}(T(k), O_m) \end{pmatrix}. \qquad (8)$$

Then, we defined an evaluation function g as:

$$g(M, T, O_m) = \sum_{k=1}^{n} \left(\sum_{i=1}^{6} \frac{|M_i(k) - f_i(T(k), O_m)|}{|M_i(k)|} \right), \quad (9)$$

which represents a scalar equivalent to the cumulative residual error between the measured currents M and the estimated currents f (for an given object O_m) along the whole trajectory. By estimating $g(M, T, O_m)$ for all O_m, the best object estimation disturbating the electric field is the object O_0 that minimizes g according to:

$$O_0 = \operatorname*{argmin}_{O_m} g(M, T, O_m). \qquad (10)$$

4.2 From an exhaustive testing to an optimized approach

The algorithm introduced in Section 4 is described in Alg. 1. It consists in systematically evaluating all the solutions, and then selecting the set of parameters that minimizes the cumulative residual error between the model and the experimental measures. As the algorithm is designed, it gives in any case a solution after browsing all the parameter space and testing all parameters combinations (the evaluation of a single candidate includes the computation of a tensor followed by a multiplication of matrices with a maximum dimension of 4). However, the exhaustive testing

input : n number of point of the trajectory
input : T the robot trajectory
input : M the measured currents along the trajectory
input : $\epsilon_{xy}, \epsilon_\theta, \epsilon_{ab}$ the discretization parameters
output: $x_0, y_0, \theta_0, a_0, b_0, \sigma_0$ characterizing an ellipsoid.

/* Stage 1: Detect object and find σ_0, side */
$t \leftarrow 0$;
while $M(t, 4) = 0$ **do**
    $t+ = 1$;
end
if $M_{t,4} > 0$ **then**
    $\sigma \leftarrow 1e5$;
    if $I_{t,1} > 0$ **then**
        side $= -l_F$;
    else
        side $= l_F$;
    end
else
    $\sigma \leftarrow 1e-5$;
    if $I_{t,1} > 0$ **then**
        side $= l_F$;
    else
        side $= -l_F$;
    end
end
/* Stage 2: Find $x_0, y_0, \theta_0, a_0, b_0$ */
/* Create candidates base */
$m \leftarrow 0$;
for $x \leftarrow -l_F$ *to* l_F *by* ϵ_{xy} **do**
    for $y \leftarrow 0$ *to side by* ϵ_{xy} **do**
        for $\theta \leftarrow 0$ *to* π *by* ϵ_θ **do**
            for a, $b \leftarrow 0$ *to* $\frac{l_F}{4}$ *by* ϵ_{ab} **do**
                $m+ = 1$;
                $O_m.score = 0$;
                $O_m.params =$ set_params $(x, y, \theta, a, b, \sigma_0)$;
                $O_m.tensor =$ eval_tensor (θ, a, b, σ_0);
            end
        end
    end
end
/* Evaluate all the candidates */
while $(|M(t, 4)| > 0) \&\& (t < n)$ **do**
    for $k \leftarrow 1$ *to* m **do**
        for $i \leftarrow 1$ *to* 6 **do**
            $O_k.score+ = |M(t, i) - f_i(T_t, O_k.params))|$;
        end
    end
end
/* Select the best candidate */
$O_m =$ sort_least_to_greatest_score(O_m);
return $O_0.params$;

Algorithm 1: Global algorithm: Ellipse localization and shape estimation from a moving underwater robot.

of all candidates is time consuming. The complexity only depends on the space discretization parameters $\epsilon_{xy}, \epsilon_\theta, \epsilon_{ab}$, as their intervals are fixed by the sensor length: $[-l_F, l_F]$ for x_0, y_0, $[0, l_F/4]$ for a_0, b_0, and $[0;\pi/2]$ for θ_s. To compute the complexity we will suppose $\epsilon_\theta = 10°$ (i.e. a constant), $\epsilon_{xy} = \epsilon_{ab}$, and we will call X the number of samples in the interval $[0, l_F/4]$ (i.e. $X = l_F/\epsilon_{xy}$). Then, the complexity can be expressed as:

$$\begin{aligned} nb &= (8X).(4X).(10).(C_X^2) \\ &= (8X).(4X).(10).(X!/(2!(X-2)!) \\ &= (8X).(4X).(10).(X.(X-1).\cancel{(X-2)!})/(2.\cancel{(X-2)!}) \\ &= (160)X^4 - (160)X^3 \end{aligned}$$

where C_X^2 is the binomial coefficient estimating all the combinations of the two semi-axis parameters without repetition since $a_0 \geq b_0$. For example, with our robot, $l_F = 22$cm with $\epsilon_{xy} = \epsilon_{ab} = 1$mm (which seems to be a desirable accuracy) the number of candidates reaches $1.29e^9$. To reduce the number of operations and improve the performance of our algorithm, we developed an optimized approach that drastically reduces the number of operations while keeping the same performance. This optimized approach is an iterative procedure that consists of 3 stages. We begin by localizing and estimating a sphere (only 3 parameters: x_0, y_0 and radius a_0). Then, from the first approximation of the sphere, we localize and roughly estimate an ellipse. Finally, from this approximated ellipse we reduce again all the intervals and increase the accuracy to the desired one. Assuming again $\epsilon_\theta = 10°$, and keeping the definition of X. The parameters intervals and accuracies at each of the steps are defined such as:

- $x_0 \in [-l_F, l_F]$, with a grid of $4X$, $y_0 \in [0, l_F]$, with a grid of $2X$ and $a_0 \in [0, l_F/4]$, with a grid of $X/4$ (rough approximation of a sphere),
- $x_0, y_0 \in [-l_F/2, l_F/2]$, with a grid $2X$ and $a_0, b_0 \in [-l_F/8, l_F/8]$, with a grid of $X/2$ (rough approximation of an ellipse),
- $x_0, y_0 \in [-l_F/8, l_F/8]$, with a grid X and $a_0, b_0 \in [-l_F/16, l_F/16]$, with a grid of $X/2$ (accurate approximation of an ellipse).

The complexity at each stage is computed as:

- $nb_1 = (4X).(2X).(X/4)$ - Rough sphere,
- $nb_2 = (2X).(2X).(4).(C_{X/2}^2)$ - Rough ellipse,
- $nb_3 = (X).(X).(10).(C_{X/2}^2)$ - Accurate ellipse,

Then, the overall complexity can be written as Eq. 4.2.

$$\begin{aligned} nb &= nb_1 + nb_2 + nb_3 \\ &= 2X^4 + 8X.(X/2).(X/2-1) + 5X^2(X/2).(X/2-1) \\ &= 2X^4 + 2X.(X).(X-2) + 5/4X^2(X).(X-2) \\ &= (13/4)X^4 - (9/2)X^3 \end{aligned}$$

This strategy reduces dramatically the number of candidates evaluated as this number is reduced to $5.5e^7$ for an accuracy of 1mm.

5. EXPERIMENTAL RESULTS

5.1 Presentation of experiments

To validate our object localization and estimation method we performed a large set of experiments in a 1m^3 tank with the slender shape robot presented in the Section 1. All experiments were performed under the same conditions: a straight line trajectory of about 40cm, and one object situated in the middle of the trajectory at a distance d (see Fig. 2). In these conditions, we experiment on 4 objects: 2 ellipsoids shapes (33×16mm and 27×18mm) with 2 different electric conductivity each (aluminum that is conductive and plastic that is insulating), 4 different angles with respect to the trajectory ($0°, 30°, 60°, 90°$), and 7 different distances ($d = 50, 60, 70, 80, 90, 100, 110$mm). In total, we performed 108 experiments instead of 112, because for each object at 50mm and 90° the robot was colliding the object. All results were obtained post-processing the raw experimental data with ©Matlab on a desktop computer equipped with an ©Intel Core i5 3.3 GHz CPU and 8 Go of RAM. Globally, the average processing time was around 10 min for an average experiment time of 3 min.

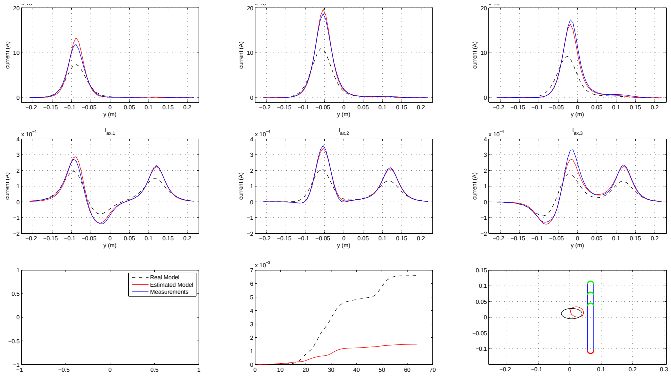

Fig. 4. Experiment using Ammari tensor with a conductive ellipsoid 33×16mm with $\theta_s = 90°$, $d = 70$mm. 1) $I_{lat,1}$ 2) $I_{lat,2}$, 3) $I_{lat,3}$ 4) $\delta I_{ax,1}$ 5) $\delta I_{ax,2}$, 6) $\delta I_{ax,3}$, 7) Legend 8) Scores 9) Result.

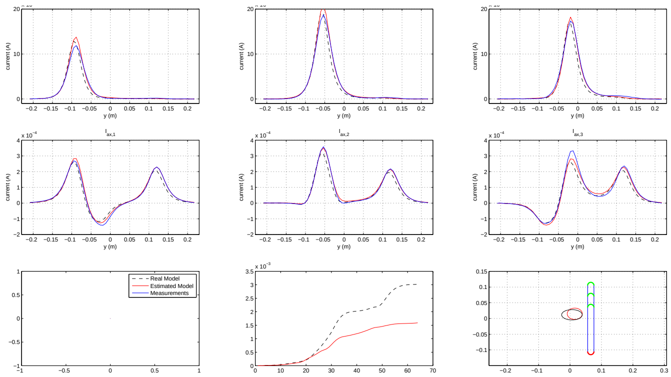

Fig. 5. Experiment using our new tensor with a conductive ellipsoid 33×16mm with $\theta_s = 90°$, $d = 70$mm. 1) $I_{lat,1}$ 2) $I_{lat,2}$, 3) $I_{lat,3}$ 4) $\delta I_{ax,1}$ 5) $\delta I_{ax,2}$, 6) $\delta I_{ax,3}$, 7) Legend 8) Scores 9) Result.

5.2 Results with the ellipsoid tensor [Ammari et al., 2014]

In Tab. 1, we present the mean results over the 108 experiments using the dipolar tensor of [Ammari et al., 2014]. This table summarizes errors on both x and y-axis in mm, on the orientation in degrees, and on the shape in percentage of shape error. This shape error is defined in Eq. 11.

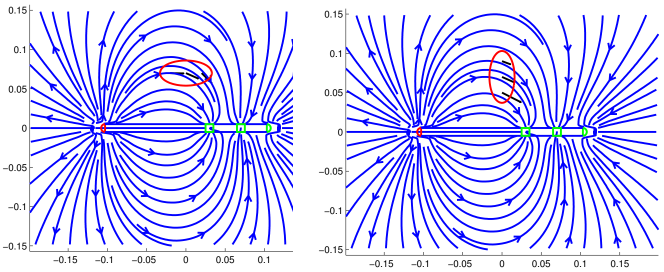

Fig. 6. Robot electric field applied on an object depending on its orientation. Up) $\theta_s = 0°$, Down) $\theta_s = 90°$. The black vectors show the orientation of the electric field in the 2 focus and in the center of an ellipse.

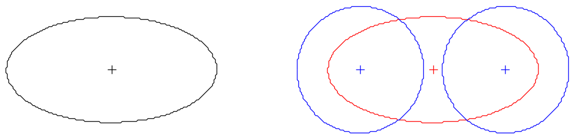

Fig. 7. The 3 objects defining the new tensor (right) compared to the nominal tensor of the ellipse (left).

$$E_s = \sqrt{\frac{(a-a_0)^2 + (b-b_0)^2}{(a^2+b^2)}}. \tag{11}$$

Moreover, we add the average processing time in minutes for a single experiment. Globally, errors are smaller on the localization than on the shape and the orientation. Moreover, errors are more important on insulating objects than on conductive objects. These errors are mainly due to the violation of an assumption on which is based our analytical model. In [Boyer et al., 2012] we suppose that the object was small enough ($a_0 \leq r_F$ with $r_F = 1$cm) to consider the electric field uniform on its domain. But, in this paper, we experiment on objects bigger than 1cm as their length is about $6.r_F$ (our biggest object is 6.6cm long). In fact, this unconsidered assumption is not problematic when the object and the sensor are aligned, i.e. $\theta_s = 0$ as the electric field is globally uniform over the object in this case (see Fig. 6.a). Unfortunately, when the angle θ_s increases towards $\pi/2$, the non uniformity of the electric field is more visible (see Fig. 6.b) and causes an underestimation of the amplitude of the estimated I_{lat} and δI_{ax}. This can be seen on Fig. 4 which reproduces experiments shown Fig. 3 after increasing θ_s to $\pi/2$. Because localization and shape are intricately linked in the electric measurements, this modelization error unavoidably leads to important errors on the object localization and on the shape estimation. It has to be noted that this phenomenon appears for both conducting and insulating object and that it increases with θ_s. To overcome this underestimation of the amplitude, we proposed a corrected tensor suited to bigger objects. This tensor models objects by 3 dipoles instead of one (1 ellipse and 2 spheres, see Fig. 7) to take into account the non uniformity of the electric field on the object (Fig. 6. b).

5.3 A new tensor for our analytical model

This new tensor consists in computing a 2 spheres electric responses superimposed to the ellipse electric response (see Fig. 7). The 2 spheres parameters (localization x_1, y_1, x_2, y_2 and 2 radius r_1, r_2) depends on the ellipse localization and size (x, y, a, b) and are obtained such as:

$$\forall i \in [1,2], \quad \begin{aligned} x_i &= x + ((-1)^i.0.8.\sqrt{(}a^2+b^2)), \\ y_i &= y, \\ r_i &= b + \frac{a}{10}. \end{aligned} \tag{12}$$

The estimated currents are modeled as a weighted sum between the ellipse currents (M_{ell}) and the 2 spheres currents (M_{sph1} and M_{sph2}) using Eq. 13.

$$M = (1-\mu).M_{ell} + \frac{\mu}{2}.(M_{sph1} + M_{sph2}). \tag{13}$$

The weights depend on the angle θ_s and the electric conductivity of the object according to Eq. 14 and 15. The weights are computed as:

$$\mu \begin{cases} [0;\frac{\pi}{2}] \to [0;1] \\ \theta_s \mapsto 1 - \frac{2}{\pi}.|\theta_s| \text{ for conducting object.} \end{cases} \tag{14}$$

$$\mu \begin{cases} [0;\frac{\pi}{2}] \to [0;\frac{1}{2}] \\ \theta_s \mapsto \frac{1}{2} - \frac{1}{\pi}.|\theta_s| \text{ for insulating object.} \end{cases} \tag{15}$$

It has to be noted that the parameters of the corrected tensor have been identified empirically on few experiments in order to complement the underestimated signal due to big objects. Using this correction, in the conditions of Fig. 4, it can be seen on Fig. 5 that the estimated currents I_{lat} and δI_{ax} and the measurements are closer to each other. To clearly show the advantage of such a correction, we compare in Tab. 1 the mean results for the shape, the orientation and the localization obtained along our 108 experiments described at the beginning of this section. Tab. 1 shows that the results are improved, as we gain in average: 2.2% on the shape errors, $3-4$mm on the localization and 2° on the orientation. This global improvement is even more visible on the shape error histogram presented on Fig. 9.a. Tab. 1 also shows that the results are a bit better for conducting objects than insulating objects but one can see that our corrected tensor is more beneficial for insulting object with an improvement of 3.5% on the shape instead of 1%.

Now, to clearly illustrate the effectiveness of localization and shape estimation algorithm we show on Fig. 8 the results on 54 experiments that is to say half of the results: real objects are plotted in red, and the corresponding estimated objects are plotted in blue. On this figure, it can be seen that for both objects, results are getting worst (localization and position) as the distance increases since in this case the signal-to-noise ratio decreases. The errors that remain on the localization and on the shape are due to the fact that both are linked in the measurements. In fact, multiple couples (object/localization) produce exactly the same measurements, thus, the algorithm sometimes cannot distinguish between a small object situated close from a bigger situated further. As a consequence, to complement these results and evaluate our algorithm and model, we performed 2 additional experiments that consist in estimating the shape when the localization x_0, y_0 is supposed known (resp. estimating the localization assuming the shape a_0, b_0 is known). Experiments for the 2 particular cases are presented on Fig.10.a and 10.b. Remarkably, results are really good in both cases even for long distances

	Loc. and shape estimation			
Params	$\epsilon_a, \epsilon_b(m)$	$\epsilon_\theta(°)$	$\epsilon_x, \epsilon_y(m)$	
Values	0.001	10	0.001	
	Nominal model			
Errors	E_s (%)	θ (°)	x (m)	y (m)
All obj.	**20.37**	**25.80**	**0.0107**	**0.0113**
Conductive	18.01	24.01	0.0094	0.0076
Insulating	22.73	27.58	0.0121	0.0151
Time	9.5 min / experiment			
	New model			
Errors	E_s (%)	θ (°)	x (m)	y (m)
All obj.	**18.48**	**24.32**	**0.0103**	**0.0010**
Conductive	17.13	26.69	0.0099	0.0076
Insulating	19.82	21.96	0.0106	0.0137
Time	10.3 min / experiment			

Table 1. Object localization and shape estimation. Mean on 108 experiments: 4 objects, 4 orientations at 7 distances.

	Shape giving loc.		Loc. giving shape		
Params	$\epsilon_a, \epsilon_b(m)$	$\epsilon_\theta(°)$	$\epsilon_x, \epsilon_y(m)$		$\epsilon_\theta(°)$
Values	0.001	10	0.002		10
	Nominal model				
Errors	E_s (%)	θ (°)	x (m)	y (m)	θ (°)
All obj.	18.59	23.79	0.0049	0.0085	29.59
Conductive	14.03	18.21	0.0051	0.0098	21.51
Insulating	23.15	29.36	0.0048	0.0072	37.66
	New model				
Errors	E_s (%)	θ (°)	x (m)	y (m)	θ (°)
All obj.	15.28	19.24	0.0043	0.0084	21.55
Conductive	11.48	11.88	0.0049	0.0102	21.96
Insulating	19.08	26.60	0.0037	0.0067	21.15
Time	1.23 min / expe.		1.02 min / experiment		

Table 2. Shape estimation giving the localization and object localization giving the shape. Mean on 108 experiments.

when the signal-to-noise ratio is very low. This is trivially explained by the fact that we estimate 3 parameters instead of 5 which reduces a lot the number of candidates. To see globally this result on the 108 experiments we show on Fig. 9.b the shape error histogram with the nominal model and the new one estimating the shape with the knowledge of the localization. This histogram shows again a global decrease of 3% of the shape errors which demonstrates the improvements brought by the new model.

6. CONCLUSION AND FUTURE WORK

We demonstrate in this paper that an underwater robot equipped with electric sense can estimate at the same time the pose and the geometric properties of an object while navigating in its surroundings. We built an algorithm that: first detects the object, then finds its electric nature and the side of the object with respect to the robot and, finally, estimates the pose and the object shape. Our algorithm has been tested on 4 different big objects with 2 different electric conductivity, 4 different orientations and at 7 distances. We obtain as average 18% of errors on the shape, 25 degrees on the orientation and less than 1cm over 108 experiments. The observed errors are mainly due to 2 factors that will be explored in future work. First inaccuracies of the model remain, in particular we still neglect the polarization of the sensor by the object and this phenomena has to be taken into account for the big objects we used. Secondly, the trajectory we chose is sometimes not discriminative enough to estimate with accuracy the object localization and geometric properties. As an example in nature, the electric fish approach the object and turn around it to estimate its pose and shape. In our future work we plan to enrich the sensing information by following more complex trajectories. For example, we will try to mimic the trajectory of the fish by navigating towards the object and turning around it. This will be achieved by using reactive behavior based on electric sense recently presented in [Lebastard et al., 2016].

REFERENCES

Ammari, H., Garnier, J., Kang, H., Lim, M., and Yu, S. (2014). Generalized polarization tensors for shape description. *Numerische Mathematik*, 126(2), 199–224.

Bai, Y., Snyder, J., Silverman, Y., Peshkin, M., and MacIver, M. (2012). Sensing capacitance of underwater objects in bio-inspired electrosense. In *IEEE/RSJ Int. Conf. on Intelligent Robots and Systems*.

Boyer, F., Gossiaux, P., Jawad, B., Lebastard, V., and Porez, M. (2012). Model for a sensor bio-inspired from electric fish. *IEEE trans. on robotics*, 28(2), 492–505.

Bullock, T. and Heiligenberg, W. (1986). *Electroreception*. Wiley Editions.

Caputi, A., Budelli, R., and Bell, C. (1998). The electric image in weakly electric fish: physical images of resistive objects in gnathonemus petersii. *Journal of Experimental Biology*, 201(14), 2115–2128.

Dimble, K.D., Faddy, J.M., and Humbert, J.S. (2014). Electrolocation-based underwater obstacle avoidance using wide-field integration methods. *Bioinspiration and Biomimetics*, 9(1).

Khairuddin, T.K.A. and Lionheart, W.R.B. (2016). Characterization of objects by electrosensing fish based on the first order polarization tensor. *Bioinspiration and Biomimetics*, 11(5), 055004.

Lanneau, S., Lebastard, V., and Boyer, F. (2016). Object shape recognition using electric sense and ellipsoid's polarization tensor. In *In Proceedings of the IEEE International Conference on Robotics and Automation (ICRA)*, 4692–4699.

Lebastard, V., Boyer, F., and Lanneau, S. (2016). Reactive underwater object inspection based on artificial electric sense. *Bioinspiration and Biomimetics*, 11(4), 045003.

Lissmann, H.W. and Machin, K.E. (1958). The mechanism of object location in *Gymnarchus Niloticus* and similar fish. *Journal of Experimental Biology*, 35(2), 451–486.

Rasnow, B. (1996). The effects of simple objects on the electric field of apteronotus. *Journal of Comparative Physiology A*, 3(178), 397–411.

Servagent, N., Jawad, B., Bouvier, S., Boyer, F., Girin, A., Gomez, F., Lebastard, V., and Gossiaux, P.B. (2013). Electrolocation sensors in conducting water bio-inspired by electric fish. *IEEE Sensor Journal*, 13(5), 1865–1882.

Truong, N., Shoukry, Y., and Srivastava, M. (2015). Bio-inspired underwater electrolocation through adaptive system identification. In *2015 American Control Conference (ACC)*, 4473–4478.

von der Emde, G., Schwarz, S., Gomez, L., Budelli, R., and Grant, K. (1998). Electric fish measure distance in the dark. *Letters to Nature, Nature*, 395, 890–894.

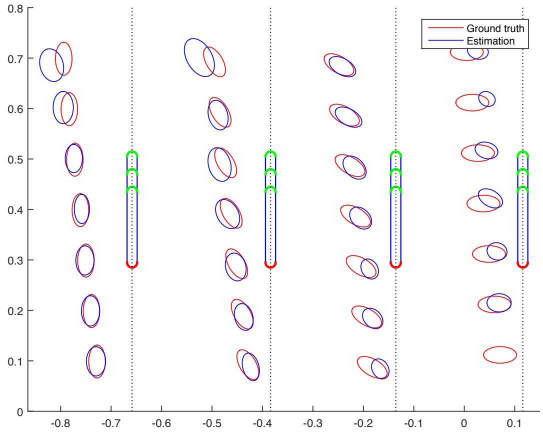

(a) Conductive ellipsoid 33 × 16mm (27 experiments)

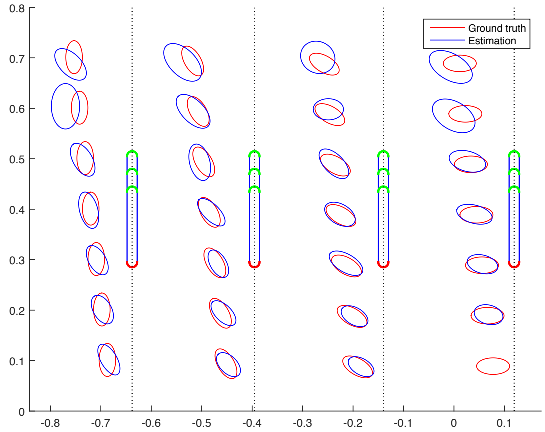

(b) Insulating ellipsoid 33 × 16mm (27 experiments)

Fig. 8. Object localization and estimation with the new tensor for 2 different object, 4 orientations, 7 distances.

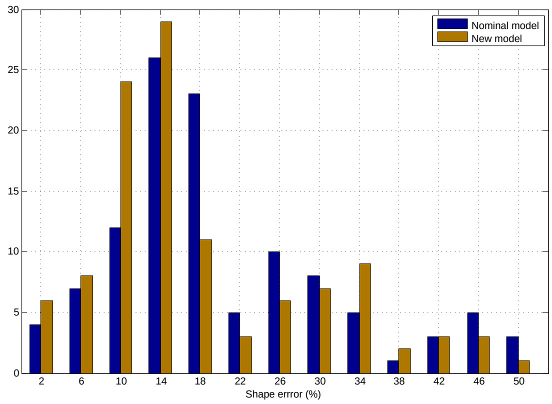

(a) Object localization and shape estimation

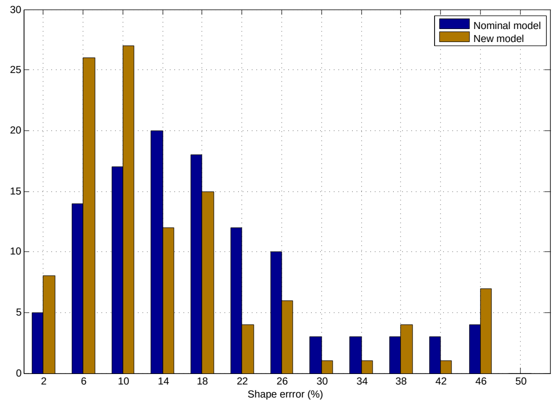

(b) Shape estimation with the knowledge of the localization

Fig. 9. Histograms of the shape error for the 108 experiments: Nominal model (blue), New model (red).

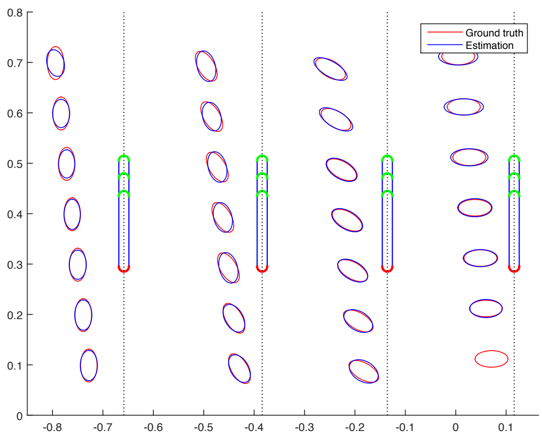

(a) Conductive ellipsoid 33 × 16mm (27 experiments)

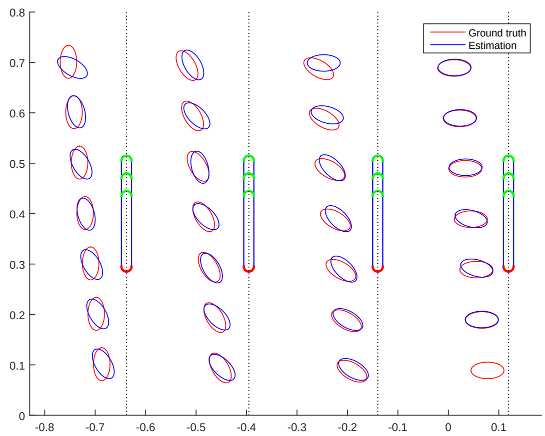

(b) Insulating ellipsoid 33 × 16mm (27 experiments)

Fig. 10. Shape estimation giving the localization (left) and object localization giving the shape (right). Both results are obtained using the new tensor.